1 Curbing Chain Transfer in initiated Chemical Vapor

2 Deposition (iCVD) via Molecular Vapor Complexation

- 3 Pengyu Chen^a, Zheyuan Zhang^a, Kwang-won Park^a, Christina H Yu^b, Rong Yang^{a,*}
- ^{a.} Robert Frederick Smith School of Chemical and Biomolecular Engineering, Cornell University,
- 5 Ithaca, NY, 14853, USA
- 6 b. Materials Science and Engineering, Cornell University, Ithaca, NY, 14853, USA
- 7 * Corresponding author: ryang@cornell.edu

Abstract

8

9

10

11

12

13

14

15

16

17

18

19

20

21

22

23

24

25

26

27

28

29 30

31

32

33

34

35

36

Initiated Chemical Vapor Deposition (iCVD) has revolutionized the preparation of high-quality conformal polymer films with excellent control over composition and properties at the nanoscale. It is compatible with over 70 functional monomers. Despite that chemical versatility, side reactions during iCVD are not well understood. For example, chain transfer could happen during the propagation of an important class of monomers that contain nitrogen (N), arresting the polymerization and limiting the molecular weight. Here, we use 1-vinylimidazole (1VI) to demonstrate that chain transfer reaction (to the imidazole group) during iCVD, which leads to unpredictable deposition kinetics, low molecular weight, and undesirable products. We further introduce a strategy that utilizes a vapor solvent to engineer monomer reactivity and suppress side reactions. By replacing the traditional patch flow, Ar, with acetic acid (AcOH), which forms hydrogen bonding with 1VI, chain transfer is suppressed, and the deposition rate is increased by as much as 280% while restoring its linear dependence on the monomer partial pressure. That linear dependence has not been achieved previously for 1VI. The tunable deposition kinetics, in turn, lead to a broader range of attainable material properties, including nearly doubling the maximum attainable molecular weight (from 7 kDa to 12 kDa) and increasing elastic modulus (from 3.5 to 4.7 GPa). The vapor solvent is also effective at suppressing chain transfer in other N-containing monomers, like (2-dimethylamine) ethyl methacrylate (DMAEMA), leading to a considerable increase in the molecular weight (from 16 kDa to 38 kDa). The vapor solvent selectively increases the reactivity of N-containing monomers during copolymerization, demonstrated using 1VI and divinyl benzene (DVB) or 1,3,5,7-tetravinyl tetramethylcyclotetrasiloxane (V4D4), increasing the reactivity ratio of 1VI by an order of magnitude according to the Fineman-Ross equation. This robust strategy engineers monomer reactivity without the need for chemical modifications. It improves the chemical precision of iCVD polymerization, particularly for an important class of N-containing monomers, which have found broad applications as the polymer-electrolyte interphase in batteries, antifouling coatings in food and water production, and bioactive and functionalizable coatings in sensors.

Keywords: initiated chemical vapor deposition, vapor solvent, Nitrogen-containing monomers, vinylimidazole, engineering reactivity, copolymerization, material property control

Introduction

Chemical vapor deposition (CVD) polymerization offers precise synthesis of polymer nanolayers with high purity. While polymer thin films/coatings are predominantly synthesized and subsequently processed using solution-based methods, such as spin-coating or ink-jet printing, CVD polymerization synthesizes polymers and forms a thin film in a single step. It is particularly suitable for polymers with limited solubility, such as crosslinked polymers, or when the solvent is incompatible with the application due to their toxicity or damage to the substrate^{1, 2}. CVD produces pinhole-free and conformal coverage, as the undesirable surface tension effects, which can cause dewetting, liquid bridging, liquid thinning, and meniscus formation during solution coating processes,³ are absent in CVD.

Among existing CVD polymerization techniques, initiated CVD (iCVD) distinctly enables chain-growth synthesis with nearly 100% retention of organic functional groups⁴. To date, it has led to over 70 functional polymer thin films. These high-purity and pinhole-free films are ideal for optoelectronic devices^{5, 6} (e.g., low-leakage-current dielectric layers) and perm-selective layers for molecular separations.⁷ The high density of reactive organic moieties at the surface augments smart behavior in active materials and soft robotics⁸ and enables post-deposition functionalization with biomolecules and nanoparticles⁹.

Despite that chemical versatility, side reactions during iCVD are poorly understood, 10 with the important example of a class of Nitrogen(N)-containing precursors, including N-vinyl monomers and methacrylate with N-containing functional group. N-containing polymers have garnered special attention in the past decade due to their unique electron-rich structure and bioactivity, making them suitable for bio-active interfaces and antifouling coatings. 11, 12 However, solution-based polymerization research has revealed that chain transfer could occur during the propagation of N-containing monomers, bringing abnormal polymerization kinetics (with either accelerated or sluggish deposition) and limiting the molecular weight¹³⁻¹⁶. Taking 1-vinylimidazole (1VI) as an example, the propensity to chain transfer is rooted in the unstable electron-rich radicals that form upon activation (e.g., as manifested by the low Q-e values), ^{17, 18} which tend to undergo chain transfer to form radicals stabilized by imidazole group. The imidazole-based radicals, as "dead" radicals, in turn, arrest propagation and limit the polymer chain length. 19-21 Similar process occurs with aminecontaining monomer, except that it forms amine-based active free radicals²². While the slow deposition rate and small molecular weight associated with 1VI are well documented¹⁵, there is a dearth of fundamental understanding of those effects in the context of CVD polymerization.

This report addresses that knowledge gap and explores strategies to mitigate chain transfer during propagation in iCVD, using 1VI as an example. While traditional iCVD leads to low molecular weight (~7 kDa) and low deposition rate (< 3nm/min) for

poly(1VI) (p1VI), replacing the traditional patch flow, Ar, with acetic acid (AcOH) increases the deposition rate and molecular weight by 2-3-fold. Those effects were attributed to the acid-base reaction between 1VI and AcOH, which suppresses the chain transfer during propagation. The tunable deposition kinetics, in turn, lead to a broader range of attainable material properties, such as elastic modulus (from 3.5 to 4.7 GPa). The strategy of leveraging vapor-phase solvation¹⁶ (i.e., hydrogen bond formation in vapor phase and acid-base reaction at interface) to suppress chain transfer is also effective for other N-containing monomers, like (2-dimethylamine) ethyl methacrylate (DMAEMA), leading to a considerable increase in the molecular weight (from 16 kDa to 38 kDa).

 During copolymerization, the aforementioned side reactions can also lead to a low reactivity ratio, hence limited incorporation of N-vinyl monomers. This makes incorporating N-containing functional moieties challenging despite their broad utility in ion-conducting and bioactive materials. For instance, the incorporation of 1VI has been reported to be capped at 55% in a crosslinked antiviral zwitterionic copolymer ²³. To address this issue, we used AcOH as the vapor solvent, which selectively enhances the surface adsorption and incorporation of 1VI, suppresses its side reactions during propagation, and improves its apparent reactivity ratio. High 1VI incorporation was achieved by copolymerizing 1VI with divinylbenzene (DVB) or 1,3,5,7-tetravinyl-1,3,5,7-tetramethylcyclotetrasiloxane (V4D4) in the presence of AcOH, lending further support to AcOH's selectively enhancement of the apparent reactivity of 1VI.

This simple strategy allows for the in-situ control of the reactions without any chemical modifications on the monomer. Modulating monomer reactivity by vapor solvent represents an unprecedentedly facile method for discovering new CVD polymer thin films, where previously unattainable film properties can be achieved by simply introducing a vaporizing solvent.

Results and Discussion

Distinct deposition kinetics of 1VI during iCVD

Traditional iCVD polymerization involves one to a few monomers and an initiator. Polymerization occurs at the surface where monomers are physisorbed, with chain initiation, propagation, and termination taking place at the gas-solid interphase²⁴. As such, the monomer surface concentration, determined by its physisorption isotherm, has been the dominating factor for controlling deposition/polymerization kinetics in iCVD. While the adsorption isotherm is often considered a function of the intrinsic chemical properties of a monomer, iCVD polymerization kinetics can be controlled systematically by tuning the monomer partial pressure over its saturation pressure, i.e., P_M/P_{sat} . The monomer surface concentration, and thus deposition kinetics, vary with P_M/P_{sat} linearly²⁵.

However, the iCVD polymerization of 1VI has been known to deviate from that linear correlation. As shown in Figure 1 (a), we confirmed that the deposition rate deviated from the linear correlation and remained at \sim 3 nm/min under $P_M/P_{sat} > 0.2$. Furthermore, the apparent activation energy for the iCVD polymerization of 1VI has been reported to be -10 kJ/mol 15 , whereas that for other iCVD monomers typically falls in the range of -60 to -160 kJ/mol $^{14, 16}$ (Figure 1 (b)). While the low deposition rate, distinct rate law, and high activation energy are unsurprising based on its unstable propagating radicals and a tendency to chain transfer 26 , these side reactions are poorly understood in the context of CVD polymerization.

Previous studies on the solution-free radical polymerization of $1VI^{19, 20}$ also captured similar zeroth-order kinetics under monomer concentrations above 2 M, which has been attributed to a degradative reaction between a propagating radical and a monomer (Figure 1 (c)). Instead of reacting with a vinyl bond, a propagating radical can attack the 2-position of the imidazole ring, resulting in a resonance-stabilized radical with no propagation capability, known as a "dead" radical. Unfortunately, the occurrence of chain transfer has rarely been captured using spectroscopy (e.g., NMR, FTIR, etc.), likely due to the subtle difference in the molecular structure. Instead, polymerization kinetics are often used to substantiate the occurrence of chain transfer 19, 27. Below, we take a similar approach to analyze the deposition kinetics to demonstrate that similar chain transfer also occurs in iCVD polymerization.

Based on the insights from solution polymerization, we derived a set of rate laws to account for potential chain transfer during iCVD of 1VI. The detailed polymerization kinetic model, which involved chain transfer, is derived in **Supplementary materials**, where we show that the polymerization was dependent on the P_M/P_{sat} under low monomer partial pressure: $\lim_{[M]\to 0} DR \sim \left(\frac{P_M}{P_{sat}}\right)^{1.5}$, where the DR is deposition rate; P_M/P_{sat} is the partial pressure of monomer over the saturation pressure of monomer under stage temperature. Furthermore, we demonstrate that the polymerization kinetics is independent of monomer concentration under high monomer partial pressure when chain transfer is included in the kinetics model: $\lim_{[M]\to\infty} DR = \frac{h_{ml}MW_Mk_pf}{2\rho k_d}$, where the h_{ml}

is the monolayer thickness of monomer; MW_M is the molecular weight of monomer; k_p

is the polymerization rate constant; f is the initiation rate; ρ is the density of polymer, and k_d is the chain transfer constant.

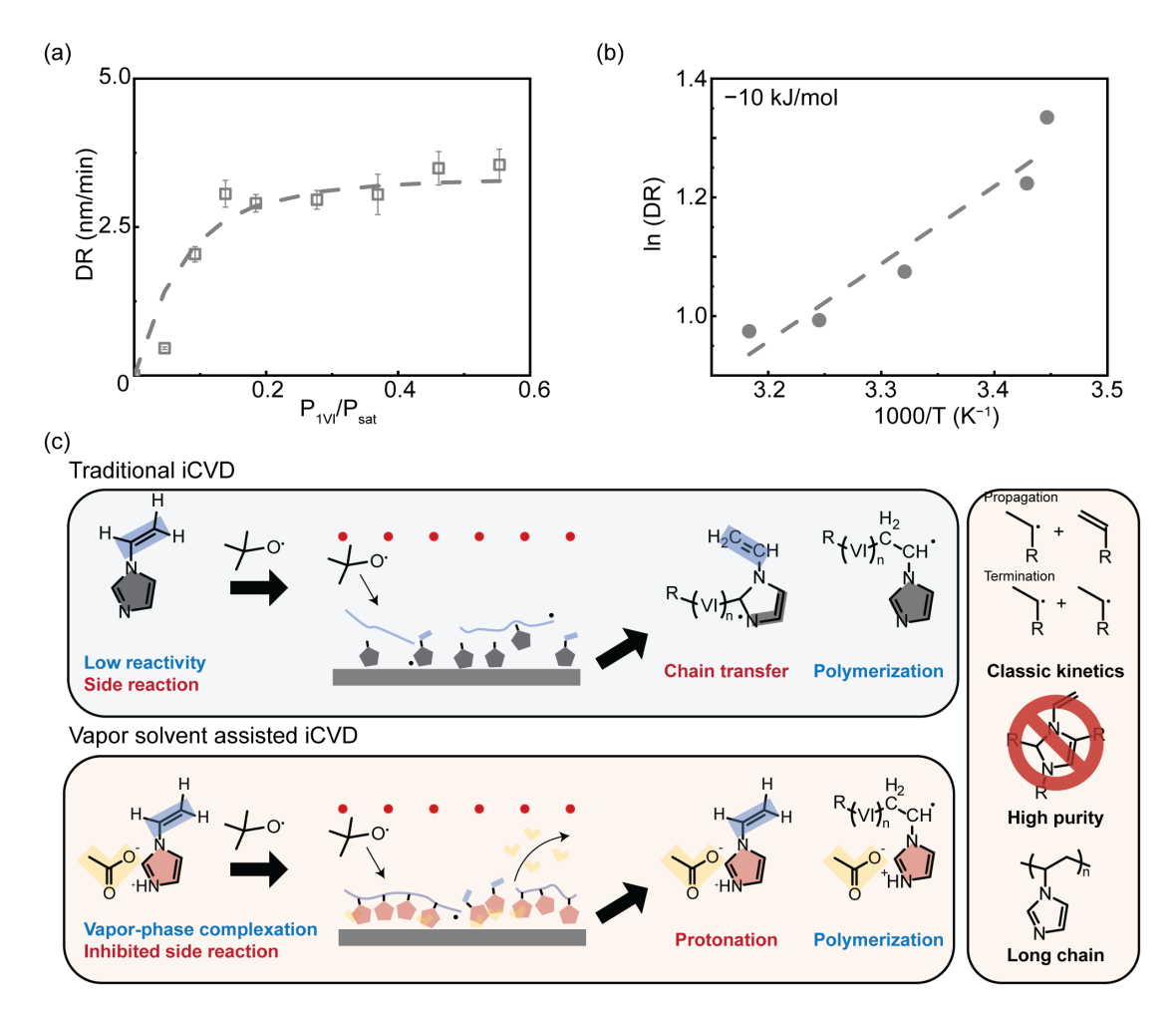


Figure 1. Demonstration of chain transfer effects causing abnormal deposition kinetics in iCVD along with a proposed mechanism for inhibiting chain transfer using vapor solvent. (a) Dependence of DR on P_{1VI}/P_{sat} under fixed total flow rates of 3 sccm, where the DR deviated from classic linear dependence. (b) The Arrhenius plot for the iCVD of p1VI, highlighting abnormal activation energy. Reproduced with permission from (15). Copyright 2024 Elsevier. (c) Schematic illustration of vapor solvent to modulate the reactivity of 1-vinylimidazole (1VI) and corresponding benefits.

<u>Inhibition of chain transfer via vapor-phase solvation of 1VI by AcOH.</u>

To inhibit chain transfer, we chose AcOH as the vapor solvent (Figure 1 (c)). We hypothesize that AcOH leads to protonation of the imidazole ring, which renders the chain transfer product energetical unfavorable and thus inhibits the side reaction.

We first confirmed the vapor-phase solvation of 1VI by AcOH by monitoring the chamber pressure as 1VI and Ar or 1VI and AcOH were co-delivered (all flow rates were 1 sccm). While 1VI and Ar followed the ideal gas law (Figure 2 (a)), 1VI and AcOH showed strong interactions, as indicated by the deviation from the ideal gas law prediction (Figure 2 (b)). The interaction was likely due to the hydrogen bonding

between 1VI and AcOH in the vapor phase.

To prevent the chain transfer reaction, it is key that the kinetics of the 1VI-AcOH complexation is faster than the kinetics of polymerization or chain transfer. The fast complexation kinetics is foreseeable based on a theoretical calculation of the collision frequency between 1VI and AcOH, using the kinetic theories²⁸. Assuming 1VI (species A) and AcOH (species B) are hard spheres, their collision frequency can be estimated as:

$$Z = N_A N_B \sigma_{AB} \sqrt{\frac{8kT}{\pi \mu_{AB}}}$$

where the Z represents the collision frequency; N_A and N_B represent molecule density of A and B, respectively; σ_{AB} represents the collision cross-section, estimated as σ_{AB} =

 $\frac{\pi}{4}(d_A + d_B)^2$, with d_A and d_B representing the molecular diameter of A and B, i.e., 0.48

12 nm and 0.4 nm for 1VI and AcOH, respectively; μ_{AB} represents the reduced mass,

estimated as $\mu_{AB} = \frac{m_A m_B}{m_A + m_B}$, with m_A and m_B representing the molar mass of A and B,

i.e., 94 Da and 60 Da for 1VI and AcOH, respectively. As such, the collision frequencies between 1VI and AcOH under different synthesis conditions are summarized in Table S1. In general, the collision frequency between 1VI and AcOH is on the order of 10^{24} - 10^{25} s⁻¹·L⁻¹. Such high frequencies, combined with the intrinsically low activation energy barrier for acid-base reactions, makes the molecular complexation fast²⁹. Furthermore, our previous work¹⁶ has illustrated that under the time scale of the experiment (i.e., a few seconds), the molecular complexation quickly reaches a thermodynamic equilibrium. Therefore, the complexation between 1VI and AcOH can be described as follows:

$$1VI(g) + AA(g) \to [1VI \cdots AA](g) \tag{1}$$

and the equilibrium can be described as:

$$\Delta P = P_{1VI\cdots AA} = KP_{1VI} \cdot P_{AA} \tag{2}$$

where K is the equilibrium constant; $P_{1VI\cdots AA}$ is the partial pressure of the 1VI-AcOH vapor complex. The equilibrium constant, K, was estimated as 13.05 ± 0.50 Torr⁻¹., similar to that of 1VI and methacrylic acid. The rapid equilibrium between 1VI and AcOH generates molecular complexes with lower volatility, enhancing the surface adsorption of complexed precursors but not the un-complexed 1VI (Figure 2 (c)).

AcOH and 1VI interact strongly enough to induce protonation of the imidazole ring and prevent chain transfer during polymerization, which was verified using nuclear magnetic resonance (NMR) spectroscopy (Figure 2 (d) and Figure S1). Upon mixing with AcOH, the hydrogen at the 2-position in imidazole shifted to low-field, indicating the protonation of C2¹⁹. That contrasts another vapor-phase solvent known to form hydrogen bonding with 1VI, i.e., hexafluoroisopropanol (HFIP), which led to chemical shifts at the 4- and 5- positions, attributed to hydrogen bonding with no protonation. Thus, the bonding nature between molecular complexes differed, although HFIP and AcOH both formed molecular complexes with 1VI.

This difference in bonding nature had different impacts on iCVD polymerization

kinetics (without changing other conditions) (Figure 2 (e)). AcOH accelerated the deposition rate by 134%, whereas HFIP, known to form a molecular complex in the vapor phase¹⁶, accelerated the deposition rate by 38%. Isopropyl alcohol (IPA) and Ar demonstrated negligible effects on the polymerization kinetics. We attributed these observations to the following effects.

1

2

3

4 5

6

7

8

9

10 11

12

13

14

15

16

17

18

19

20

21

22

23

24

25

26

27

28 29

30

31

32

33 34

35

36

37

38

39

40 41

42

43

44

For a weak Lewis acid and weak hydrogen bond donor, like IPA, its minimal effect on the deposition kinetics indicates a negligible interaction with 1VI. For a weak acid and strong hydrogen bond donor, like HFIP, its low acidity (pKa = 9) is insufficient for protonating the imidazole nitrogen and preventing the degradative chain addition. AcOH (pKa = 4.5) represents a strong hydrogen bond donor with greater acid than HFIP. Its successful restoration of the first-order kinetics can be attributed to the formation of an AcOH-1VI molecular complex in the vapor phase via hydrogen bonding, as well as the partial proton transfer (from AcOH to 1VI) upon adsorption to the surface of the substrate. Similar observations have been made in nonpolar solvents in prior studies^{30, 31}. Interestingly, using an even stronger acid, TFA (pKa = 0.2), we observed solid formation upon introducing the TFA and 1VI co-flow into the chamber (Figure S3). The opaque and birefringent appearance of this solid points to its crystalline nature, which prevents the formation of a high-quality and smooth film and the removal of the complexation partner upon completion of polymerization. As such, we believe that the interaction between an organic acid and a basic monomer should be strong enough to suppress chain transfer yet reversible enough to allow for the removal of the complexation partner, ensuring the purity of the polymer thin film. AcOH represents a favorable choice, striking a balance between effective protonation and sufficient reversibility. Below, we connect the acceleration effect of AcOH with the inhibition of chain transfer by building upon the aforementioned kinetic model.

The deposition kinetics obtained using Ar exhibited a zero-order dependence on monomer surface concentration (at $P_M/P_{sat} > 0.2$) (Figure 1 (a), replotted in Figure 2 (f) for clarity). That deviation indicates chain transfer because the classic model of iCVD kinetics predicts a linear dependence as described in Supplementary Materials. By replacing Ar with AcOH, the linear dependence was restored (Figure 2 (f)), which can be fitted as $DR_{1VI} = 34.0 \times F_{1VI} - 1.8$, where the last data point obtained at P_M/P_{sat}=0.37 was omitted because condensation of the 1VI-AcOH complex occurred (visible to the naked eye on the reactor stage). Additionally, the deposition rate increased linearly with respect to the partial pressure of AcOH when the flow rate of 1VI (F_{VI}) was fixed at 1 sccm (Figure 2 (g)), fitted as $DR_{1VI} = 11.6 \times P_{AcOH} + 3.1$. This is consistent with previously published deposition kinetics involving vapor solvation, where we demonstrated that the formation of molecular complex was linear to the partial pressure of AcOH under fixed partial pressure of 1VI¹⁶. Overall, using AcOH as the patch flow suppressed chain transfer during the iCVD of 1VI, reducing the deviation of 1VI deposition kinetics from the classical model and increasing the predictability of the deposition rate.

The protonation of 1VI by AcOH was further corroborated by a change in the apparent activation energy of iCVD. While the apparent activation energy of iCVD is negative due to the rate-limiting effect of the monomer adsorption step, protonation by

5

6

7

8

9

10

1112

13

14

15

1617

18

19

20

2122

23 24

25

26

27

AcOH, which is an exothermic process, would further decrease that activation energy. Indeed, the apparent activation energy of 1VI deposition decreased from -42.9 kJ/mol to -66.9 kJ/mol, as demonstrated using the Arrhenius plots when varying the stage temperature (Figure S3).

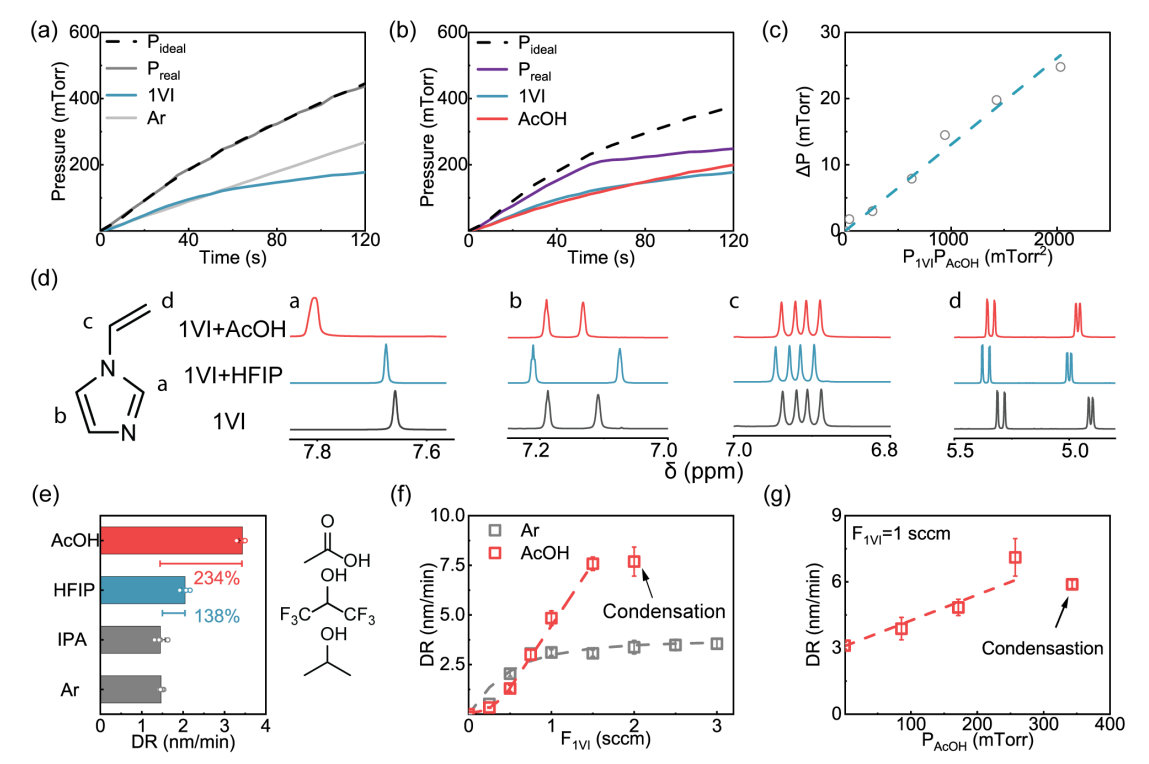


Figure 2. Rapid vapor-phase equilibrium of 1VI protonation by AcOH, which restored the classical linear dependence of deposition rate on surface monomer concentration. (a) Chamber pressure followed the prediction of ideal gas law when 1VI and Ar were co-delivered into the reactor. (b) Chamber pressure deviated from the prediction when 1VI and AcOH were co-delivered into the reactor, indicating vaporphase solvation. (c) ΔP , i.e., the difference between the experimentally measured pressure and the ideal-gas-law predictions, and $P_{IVI}P_{AcOH}$ (i.e., the product of the partial pressures) follows linear correlation, implying a rapid equilibrium with an equilibrium constant K of 13 Torr⁻¹ from a linear regression. (d) The ¹H NMR spectra of 1VI, 1VI with HFIP and 1VI with AcOH. The molar ratio of 1VI and vapor solvent is one. (e) Deposition rates (DR) of p1VI using Ar, isopropyl hexafluoroisopropanol (HFIP), and AcOH as vapor solvent under identical flow rates, total pressure, and stage temperature. (f) Dependence of DR on F_{IVI} under fixed total flow rates of 3 sccm, where the classic linear dependence on F_{IVI} was restored. F_{AcOH} was fixed at 1sccm when used. (g) The dependence of DR on P_{AcOH} under fixed F_{IVI} of 1 sccm, showing a linear increase.

Enhanced film properties by vapor solvent

To assess the effects of AcOH on the p1VI film quality and properties, p1VI films were deposited with Ar or AcOH and compared in terms of their bulk and surface properties.

The film chemistry was characterized using Fourier transform infrared spectroscopy (FTIR) and X-ray photoelectron spectroscopy (XPS). In FTIR, the peaks at 1494, 1284, 1100, and 740 cm⁻¹, corresponding to the imidazole ring in both cases¹⁵; and the intensity of the peaks at 1700 cm⁻¹ also remained unchanged, indicating no incorporation of AcOH into p1VI film. (Figure S4). Notably, the peak at 1647 cm⁻¹ (in red), which signifies the vinyl bond, was observed in the p1VI films deposited using Ar but not AcOH. This suggests that the complexation with AcOH increased the percentage conversion of the vinyl bond during 1VI polymerization, supporting its inhibitive effect on the side reaction (i.e., chain transfer to the imidazole ring). XPS showed the presence of C, N, and O in both films with similar elemental compositions (Table 1, Figure S4). The elemental compositions closely resemble the theoretical values, i.e., 71%, 28%, and 1% for C, N, and O, respectively, with the slightly higher percentages of C and O attributed to adventitious species.

Table 1. Atomic ratio of p1VI film deposited using Ar and AcOH obtained from XPS survey scan and the theoretical value.

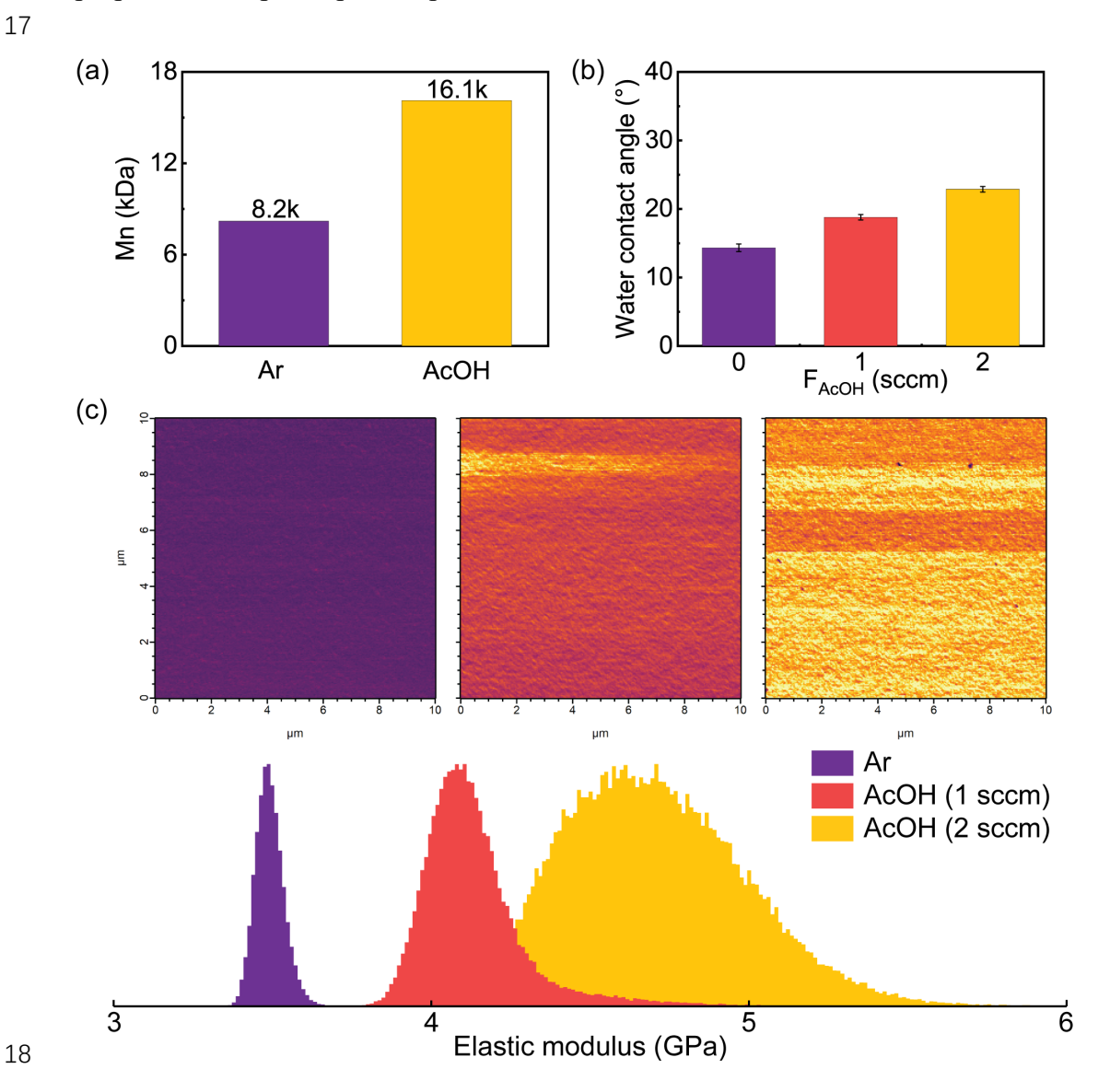
Patch flow	C (%)	N (%)	O (%)
Ar	73.6	22.2	4.2
AcOH	74.5	21.6	3.8
Theoretical	71.0	28.4	0.6
composition			

 The use of AcOH increased the molecular weight (Mw) of p1VI. The molecular weight of p1VI deposited using Ar, measured with gel-permeation chromatography (GPC), was 8.2 kg/mol. By replacing Ar with AcOH, the molecular weight increased to 16.1 kg/mol (Figure 3 (a)). The polydispersity indexes (PDI) were 1.24 and 1.34 for the Ar and AcOH depositions, respectively. The increased molecular weight was likely due to the collective effects of enhanced surface adsorption of 1VI and the inhibition of chain transfer in the presence of AcOH.

The surface energy of the p1VI films was characterized by water contact angle (WCA) measurements. A series of p1VI films were deposited with a constant flow rate of the patch flow, i.e., 2 sccm, but varying compositions of Ar and AcOH (Figure 3 (b)). The WCA of p1VI deposited using pure Ar was 14.3±0.5°. By replacing 1 sccm Ar with AcOH, the WCA increased slightly to 18.8±0.4°, and it further increased to 22.9±0.4° when using 2 sccm AcOH. The increased WCA on films obtained using AcOH was likely a result of the suppressed chain transfer. While WCA has been observed to increase with molecular weight due to greater dispersive forces at higher molecular weights³², that increase is usually limited to a few degrees. The observed increase (~10°) thus likely reflects the influence of the suppressed chain transfer. The degradative addition disrupts the imidazole ring, forming two hydrophilic amine groups and leading to a lower WCA. As we suppress the degradative addition, we increase the WCA and the fraction of intact imidazole rings simultaneously, leading to the apparent positive correlation between molecular weight and WCA.

Bimodal atomic force microscopy (bimodal AFM) was used to simultaneously

characterize the surface morphology and elastic modulus (E). All p1VI films exhibited a smooth surface with root-mean-square (RMS) roughness of 0.35±0.05, 0.35±0.06, and 0.24±0.02 nm, respectively, when using 0, 1, and 2 sccm AcOH was used (while keeping the total patch flow rate at 2 sccm) (Figure S5). However, E differed significantly, varying from 3.49±0.04 GPa to 4.1±0.11 GPa, to 4.67±0.29 GPa (all with Gaussian distribution) when 0, 1, and 2 sccm AcOH was used (Figure 3 (c)). The greater mechanical strength exhibited by p1VI films deposited with a greater amount of AcOH was likely a result of their higher molecular weight, and thus, less defect from the chain ends, a greater degree of chain entanglement, and reduced chain relaxation. The latter can be estimated based on the anticipated increase in T_g by ~11°C as the molecular weight increases from 8.2 kDa to 16.1 kDa, calculated using the Flory-Fox equation (see Supplementary Materials for detailed calculation). For polymers with molecular weight less than 10 kDa, an increase in T_g has been shown to significantly enhance the elastic modulus.^{33, 34} Taken together, our results show that using AcOH as a vapor solvent can significantly enhance the purity, molecular weight, and mechanical properties of vapor-deposited p1VI films.



1

2

3

4

5

6 7

8

9 10

11

12

13

14

15

16

Figure 3. Enhanced p1VI film properties by AcOH vapor solvent. (a) The molecular weight (Mn) of iCVD p1VI using Ar or AcOH as the patch flow. (b) The water contact angle (WCA) of p1VI deposited using 0, 1, or 2 sccm AcOH while keeping the total patch flow rate of 2 sccm. (c) Elastic modulus mapping of the p1VI films using 0, 1, or 2 sccm AcOH, showing increasing elastic moduli, and their histograms.

Enhanced monomer reactivity during copolymerization

The chain transfer reaction and inherent low reactivity of 1VI lead to a low reactivity ratio during copolymerization, limiting the incorporation of N-vinyl monomers and rendering it challenging to incorporate N-containing functional moieties ²³. To address this issue, we demonstrate below that AcOH selectively enhances the surface adsorption and incorporation of 1VI and improves its apparent reactivity ratio (**Figure 4(a)**). We chose two common crosslinkers in iCVD for this demonstration, DVB and V4D4. We systematically varied the monomer to crosslinker ratio in the vapor-phase feed and quantified the reactivity ratios of 1VI-DVB and 1VI-V4D4 pairs using the Fineman-Ross Method:

$$\frac{f_{1VI}(2F_{1VI}-1)}{(1-f_{1VI})F_{1VI}} = \frac{r_{1VI}f_{1VI}^2(1-F_{1VI})}{(1-f_{1VI})^2F_{1VI}} - r_{DVB\ or\ V4D4}$$
(3)

where f_{IVI} is the mole fraction of 1VI in the feed, i.e., the fraction surface molar concentration of 1VI, which was calculated using the BET isotherm and the P_{IVI}/P_{sat} and P_{DVB}/P_{sat} or P_{V4D4}/P_{sat} values; F_{IVI} is the mole fraction of 1VI repeat units in the copolymer, calculated from the FTIR or XPS data; r_{IVI} is the reactivity ratio of 1VI to DVB or V4D4.

Using Ar, the 1VI-DVB pair exhibited reactivity ratios of 0.03 and 3.71, respectively, for r_{IVI} and r_{DVB} . A maximum F_{IVI} of ~ 47% was obtained with an f_{IVI} of ~90% (Figure 4(b), Figure S6 (left)). The deposition rate was capped at 3 nm/min. By simply replacing Ar with AcOH, the pair exhibited a much-increased r_{IVI} of 0.18, and a decreased r_{DVB} of 1.64 (Figure 4(c), Figure S6 (right)). With an f_{IVI} of ~90%, as much as 69% of the repeat units in the copolymer were 1VI.

The effects of AcOH were even more pronounced in the 1VI-V4D4 system. While Ar led to r_{IVI} and r_{V4D4} of 0.21 and 1.00, respectively (Figure 4(b), Figure S7 (left)) AcOH increased r_{IVI} to 1.70 and reduced r_{V4D4} to 0.34. A maximum F_{IVI} of ~ 94% was obtained at an f_{IVI} of ~90%, a one-third increase compared to the maximum F_{IVI} for Ar (i.e., ~72%) (Figure 4(c), Figure S7 (right)).

Theoretical manifestations of 1VI's unstable propagating radical and chain transfer proclivity are encapsulated by its semi-empirical Q-e parameters: Q_{1VI} =0.11 and e_{1VI} =-0.68²⁶. During copolymerization with crosslinkers such as DVB or V4D4 (referencing Q-e value for styrene (S) and vinyl triethoxysilane (V): Q_s =1 and e_s =-0.80; Q_v =0.021 and e_v =0.82³⁵, the weak resonance stabilization effect and electron-rich nature of 1VI enhance the likelihood of incorporating crosslinkers over N-containing monomers. Simultaneously, the multiple vinyl groups on the crosslinker further reinforce this tendency. In practical terms, this imposes stringent requirement on flux control, as the surface monomer concentration must be meticulously regulated to be

approximately two orders of magnitude higher in 1VI than in the crosslinker, ensuring the formation of a polymer film rich in functional groups. Moreover, the formation of "dead" radical via chain transfer readily quenches the polymerization, leading to low deposition rate of 1 to 3 nm/min.

The use of AcOH effectively mitigates the previously mentioned challenges. We attributed the enhanced incorporation of 1VI into crosslinked copolymer films to the enhanced adsorption and, thus, an increased surface concentration of 1VI upon complexation with AcOH. That effect on enhanced surface adsorption can be quantified using the derived complexation equilibrium constant, K, regressed as 13 Torr⁻¹ through Equation (2) and the saturation pressure of molecular complex, 1VI and AcOH, estimated as 0.21 Torr based on Figure 2. The effective surface monomer concentration of 1VI experiences a 3.8-fold increase upon factoring in the effects of AcOH, detailed in Supplementary Materials. Updating the surface monomer concentration leads to a correction of the surface monomer fraction, denoted as the corrected f_{IVI} , and replot the fitted curve from Figure 4(b) into Figure 4(d). Following these adjustments, r_{VI} and r_{DVB} are fitted as 0.05 and 6.21, respectively, in 1VI-DVB system, while r_{VI} and r_{V4D4} are fitted as 0.45 and 1.30 in 1VI-V4D4 system—values close to those obtained with Ar. Directly using the reactivity ratio obtained with Ar, the prediction error of film composition is merely 2%±4% for 1VI-DVB system and -9%±3% for 1VI-V4D4 system using corrected f_{IVI} , underscoring the selectively enhanced surface monomer concentration as the primary factor contributing to the heightened enhanced apparent reactivity. Any residual error can be ascribed to minor factors, including complexation effect with crosslinker, altered adsorption behavior and changed reactivity due to 1VI protonation.

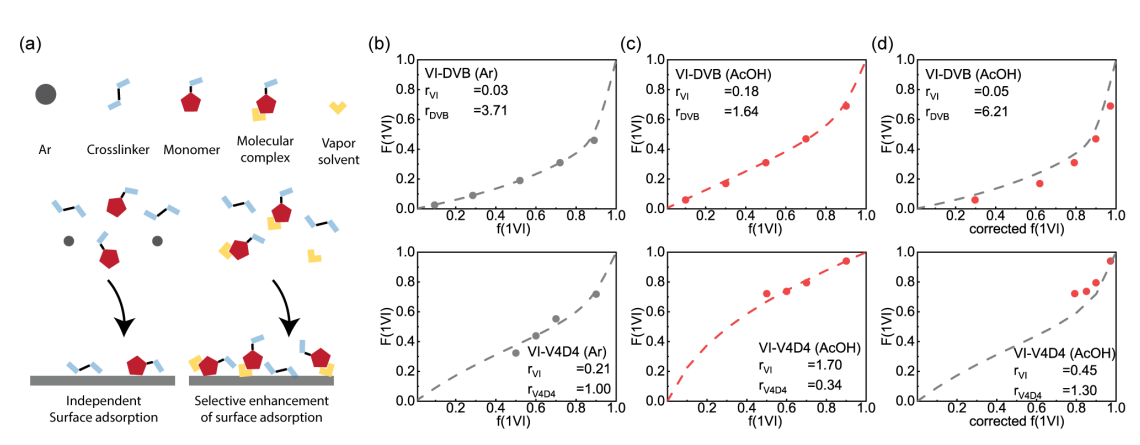


Figure 4. Enhanced apparent reactivity ratio of 1VI by AcOH during copolymerization. (a) Schematic illustration of the mechanism of selective solvation to enhance the apparent reactivity ratio of 1VI in iCVD. (b-c) The Fineman-Ross method to quantify the reactivity ratio of 1VI during copolymerization. The molar fraction of 1VI repeat units in the copolymers (F_{IVI}) was illustrated as a function of the fraction of 1VI monomer at the substrate surface (f_{IVI}). The upper panels correspond to the 1VI-DVB pair, and the lower ones are the 1VI-V4D4 pair. Data were obtained using (b) Ar and (c) AcOH. (d) The Fineman-Ross method to quantify the reactivity ratio of

1VI during the copolymerization with DVB (upper panel) and V4D4 (lower panel) after correcting for the enhanced 1VI surface adsorption due to AcOH complexation.

Generalizability of the effects of AcOH to other N-containing monomers

The need to modulate monomer reactivity is not unique to N-vinyl monomers. For instance, (2-dimethylamine) ethyl methacrylate (DMAEMA) also tends to chain transfer during propagation, as indicated by a chain transfer constant of 1.9 for methacrylate to triethylamine³⁶. This chain transfer reaction produces radicals that can propagate further, as evidenced by the auto-accelerated deposition rate and low molecular weight of the as-synthesized pDMAEMA. We observed an average deposition rate of 5.4 nm/min for a 100-nm pDMAEMA film, which increased by nearly 4-fold to 19 nm/min for a 1000-nm film under identical deposition conditions. This self-accelerating effect is likely a result of a chain transfer effect that allows the higher active free radical concentrations on the surface, thus, a high overall polymerization rate. The molecular weight (Mw) of pDMAEMA was merely 16 kDa despite the high deposition rate, whereas similar deposition rates routinely lead to molecular weights of 20–40 kDa using iCVD and other methacrylate monomers³⁷.

AcOH, as a vapor solvent, effectively suppressed the side reactions during DMAEMA depositions. The deposition rate remained constant at 9.9 nm/min for 100-nm and 1000-nm pDMAEMA films. Although the deposition rate was lower than that recorded for the 1000-nm pDMAEMA film deposited using Ar, the molecular weight increased by over 2-fold to 38 kDa (Figure S8). These results combined demonstrate that the vapor solvent of AcOH renders the deposition kinetics more predictable and the molecular weight more controllable for N-containing monomers beyond 1VI. It has the potential to expand the space of attainable material properties for iCVD functional polymers.

Conclusion

In conclusion, we have demonstrated the ability of a vapor solvent, AcOH, to suppress side reactions during the iCVD polymerization of N-containing monomers, using 1VI as an important example. AcOH inhibits chain transfer reactions during iCVD by complexing with 1VI and protonating it, which reaches rapid equilibrium in the vapor phase with an equilibrium constant of 13 Torr-1. This strategy improves the quality of p1VI thin films, leading to increased molecular weight, polymer purity, and elastic modulus. Furthermore, selective solvation enhanced the surface adsorption of 1VI, increasing their reactivity ratio during copolymerization and enabling their incorporation into crosslinked films with unprecedented molar fractions. While we demonstrated the generalizability of this strategy using DMAEMA, it could apply to other functional monomers bearing highly reactive side chains, such as thiol and amine, thus expanding the iCVD monomer library and enabling high-quality functional polymer thin films with unprecedented functions.

Materials and Methods

Initiated chemical vapor deposition (iCVD). All the polymeric thin films were synthesized using iCVD in a custom-built vacuum reactor (Kurt Lesker). Thermal activation of the initiator was provided by resistively heating a 0.5 mm nickel/chromium filament (80% Ni/ 20% Cr, Goodfellow) mounted as a parallel filament array. Filament heating was controlled by a DC power supply. The deposition stage that was kept at desired substrate temperatures using a chiller. The vertical distance between the filament array and the stage was 2 cm. Depositions were performed on Si wafers (P/Boron<100>, Purewafer). Initiator (tert-butyl peroxide (TBPO, Sigma-Aldrich, 98%)), monomers (1-vinylimidazole (1VI, Sigma-Aldrich, 99%), divinylbenzene (DVB, Sigma-Aldrich, 80%), 1,3,5,7-tetravinyl-1,3,5,7tetramethylcyclotetrasiloxane (V4D4, Ambeed, 97%), 2-(dimethylamino)ethyl methacrylate (DMAEMA, Sigma-Aldrich, 98%)) and patch flow Argon (Ar, Airgas), isopropanol (IPA, Sigma-Aldrich, 99.5%), 1,1,1,3,3,3-hexafluoro-2-propanol (HFIP, Sigma-Aldrich, 99%)), Acetic acid (AcOH, Sigma-Aldrich, 99%), were used without further purification. During iCVD, 0.5 sccm TBPO was introduced to the reactor at room temperature through a mass flow controller for all the depositions. Monomers and patch flow were heated to desired temperatures (room temperature for IPA, AcOH, HFIP; 65°C for 1VI, DVB, DMAEMA; 80°C for V4D4) in their respective glass jars to create sufficient pressure to drive the vapor delivery into the vacuum chamber.

1

2

3

4

5

6

7

8

9

10

11

12

13

14

15

16

17

18

19

20

21

22

23

24

25

26

27

28 29

30

31

32

33

34

35

36

37

38

39

40 41

42

43

44

During depositions for kinetic studies, the chamber pressure was kept at 600 mTorr, the filament array temperature was set to 230°C, and the TBPO flow rate was 0.5 sccm unless otherwise stated. Stage temperature, controlled by a cooling circulator and monitored using a thermocouple attached to the stage. For the 1VI/vapor solvent series in Figure 2 (e), the substrate temperature was kept at 30°C; the total flow rate was 3.5 sccm, with 1 sccm 1VI, 2 sccm vapor solvent. For the 1VI/Ar series in Figure 2 (f), the total flow rate was kept at 3.5 sccm, with $(0.25+0.25\times x)$ sccm 1VI, $(2.75-0.25\times x)$ sccm Ar, where x=0, 1, 2, 3, 5, 7, 11. For the 1VI/AcOH series in Figure 2 (f), the total flow rate was kept at 3.5 sccm, with 1 sccm of AcOH, (0.25+0.25×x) sccm 1VI, $(1.75-0.25\times x)$ sccm Ar, where x=0, 1, 2, 3, 5, 7. For the 1VI/AcOH series in Figure 2 (g), the total flow rate was kept at 3.5 sccm, with 1sccm 1VI, $(2-0.5\times x)$ sccm Ar, and 0.5×x sccm AcOH, where x=0, 1, 2, 3, 4. For the activation energy series, the total flow rate was 3.5 sccm, with 0.5 sccm of 1VI, 0.5 sccm of TBPO, 1.5 or 2.5 sccm of Ar, and 1 or 0 sccm of AcOH with cooler temperature setting as 10, 15, 20, 25, 30°C. For the molecular weight/water contact angle/AFM series in Figure 3, 1 sccm of 1VI, 2 sccm of patch flow that was consisted of Ar and AcOH, and 0.5 sccm of TBPO were simultaneously introduced into the reactor. The step change in flowrates was 0.25 sccm for all series, corresponding to about 40 mTorr change in the partial pressure of the species of interest.

For the deposition of copolymer, the following flow rates were used. (i) 1VIDVB(Ar or AcOH) film: $(0.2+0.4\times x)$ sccm DVB, $(1.8-0.4\times x)$ sccm 1V, 1 sccm Ar or AcOH, 0.5 sccm TBPO, where x=0,1,2,3,4; (ii) 1VI-V4D4(Ar or AcOH) film, 0.015, 0.065, 0.1, 0.15 sccm V4D4, 1 sccm 1V, 2 or 1 sccm Ar , and 0 or 1 sccm AcOH, 0.5 sccm TBPO.

For the deposition of DMAEMA polymer film, the total flow rate was 2.6 sccm,

with 0.6 sccm of TBPO, 1 sccm of DMAEMA and 1 sccm of Ar or AcOH.

In situ interferometry with a HeNe laser source (wavelength = 633 nm, JDS Uniphase) was used to monitor the film growth on a Si substrate. A more accurate film thickness on the Si wafer substrates was measured post-deposition using a J. A. Woollam Alpha-SE spectroscopic ellipsometry at three different incidence angles (65°, 70°, 75°).

Non-ideality assessment. The measurement was conducted in the customized vacuum chamber described above. The monomer and patch flow were introduced into the vacuum chamber with the flow rate of 1 sccm for each. The chamber pressure was measured using a Baratron (0-2 Torr, MKS) every 5 seconds. Each flow condition was measured at least twice to ensure repeatability.

<u>Materials characterization.</u> Fourier transform infrared (FTIR) measurements were performed on a Bruker Vertex V80v vacuum FTIR system in transmission mode. A deuterated triglycine sulfate (DTGS) KBr detector over the range of 600–4000 cm⁻¹ was used with a resolution of 4 cm⁻¹. The measurements were averaged over 64 scans to obtain a sufficient signal-to-noise ratio. All the spectra were baseline-corrected by subtracting a background spectrum of bare Si.

For XPS, samples were analyzed using a Surface Science Instruments SSX-100 ESCA Spectrometer with operating pressure ca. $1x10^{-9}$ Torr. Monochromatic Al K α x rays (1486.6 eV) with photoelectrons collected from an 800- μ m-diameter area. Photoelectrons were collected at a 55° emission angle with a source-to-analyzer angle of 70°. A hemispherical analyzer determined electron kinetic energy using a pass energy of 150 eV for wide/survey scans. All the samples were stored under vacuum at room temperature for a week before XPS analysis.

 Surface roughness and topography were measured using a Cypher S AFM. Scans were recorded across 10 \times 10 μm regions at 1.0 Hz in AM-FM mode.

 The NMR spectra were obtained using a Bruker AV500. In preparation for NMR, 2% (volume fraction) 1VI and/or AcOH, HFIP was dissolved in 600 μL chloroform-d (Aldrich, 99.9%) for ¹H analysis.

 The molecular weight of the as-deposited polymer films was characterized by gel permeation chromatography (GPC) (Waters), which was equipped with a Waters 410 differential refractive index detector. N, N-dimethylformamide (DMF) was used as the eluent at room temperature.

Data availability: All data needed to evaluate the conclusions in the paper are presented in the paper and/or the Supplementary Materials.

Supplementary Information

Supplementary information contains additional discussions on the kinetic model, the calculation of surface monomer concentration, the estimation of T_g of p1VI, supplementary data on the deposition kinetics, additional characterization data on the p1VI film from FTIR, XPS, AFM, NMR, optical image of the TFA-1VI crystalline

condensation, and additional data on pDMAEMA.

2
 3

Acknowledgment

- 4 This work was supported by the National Science Foundation Faculty Early Career
- 5 Development Program [grant number CMMI-2144171]. We also wish to express our
- 6 appreciation for KIC Graduate Fellowship at Cornell University for the support granted
- 7 to P.C.

8

- 9 Author contributions: P.C., Z.Z., and R.Y. designed the research and experiments. P.C.,
- 2.Z. conducted the depositions and characterizations. K.P. conducted AM-FM AFM.
- P.C. performed the data analysis and model development. P.C. and R.Y. drafted the
- manuscript. All authors provided critical feedback on experimental design and data
- analysis and reviewed the manuscript.

1415

Reference

- 16 1. Gleason, K. K., Designing Organic and Hybrid Surfaces and Devices with Initiated Chemical Vapor
- 17 Deposition (iCVD). Adv. Mater. 2023, 36, 2306665, DOI:10.1002/adma.202306665.
- 18 2. Qiu, M.; Du, W.; Zhou, S.; Cai, P.; Luo, Y.; Wang, X.; Yang, R.; Zhao, J., Recent
- 19 progress in non-photolithographic patterning of polymer thin films. *Prog. Polym. Sci.* **2023**, *142*, 101688,
- 20 DOI:10.1016/j.progpolymsci.2023.101688.
- 21 3. Yu, S. J.; Pak, K.; Kwak, M. J.; Joo, M.; Kim, B. J.; Oh, M. S.; Baek, J.; Park, H.;
- 22 Choi, G.; Kim, D. H.; Choi, J.; Choi, Y.; Shin, J.; Moon, H.; Lee, E.; Im, S. G., Initiated
- 23 Chemical Vapor Deposition: A Versatile Tool for Various Device Applications. Adv. Eng. Mater. 2018,
- 24 20 (3), 1700622, DOI:10.1002/adem.201700622.
- 4. Gleason, K. K., Nanoscale control by chemically vapour-deposited polymers. Nat. Rev. Phys. 2020,
- 26 2, 347–364, DOI:10.1038/s42254-020-0192-6.
- 27 5. Wang, M.; Wang, X.; Moni, P.; Liu, A.; Kim, D. H.; Jo, W. J.; Sojoudi, H.; Gleason, K.
- 28 K., CVD Polymers for Devices and Device Fabrication. Adv. Mater. 2017, 29 (11), 1604606,
- 29 DOI:10.1002/adma.201604606.
- 30 6. Huo, N.; Rivkin, J.; Jia, R.; Zhao, Y.; Tenhaeff, W. E., Synthesis of High Refractive Index
- 31 Polymer Thin Films for Soft, Flexible Optics Through Halomethane Quaternization of Poly(4-
- 32 Vinylpyridine). *Advanced Optical Materials* **2024**, *n/a* (n/a), 2302201, DOI:10.1002/adom.202302201.
- 33 7. Joo, M.; Shin, J.; Kim, J.; You, J. B.; Yoo, Y.; Kwak, M. J.; Oh, M. S.; Im, S. G., One-
- 34 Step Synthesis of Cross-Linked Ionic Polymer Thin Films in Vapor Phase and Its Application to an
- 35 Oil/Water Separation Membrane. J. Am. Chem. Soc. 2017, 139 (6), 2329-2337,
- 36 DOI:10.1021/jacs.6b11349.
- 37 8. Xiao, Y.-Y.; Jiang, Z.-C.; Zhao, Y., Liquid Crystal Polymer-Based Soft Robots. Advanced
- 38 Intelligent Systems 2020, 2 (12), 2000148, DOI:10.1002/aisy.202000148.
- 39 9. Bacheller, S.; Dianat, G.; Gupta, M., Synthesis of pH-Responsive Polymer Sponge Coatings and
- 40 Freestanding Films via Vapor-Phase Deposition. ACS Appl. Polym. Mater. 2021, 3 (12), 6366-6374,
- 41 DOI:10.1021/acsapm.1c01151.
- 42 10. Khlyustova, A.; Cheng, Y.; Yang, R., Vapor-deposited functional polymer thin films in biological
- 43 applications. Journal of Materials Chemistry B 2020, 8 (31), 6588-6609, DOI:10.1039/D0TB00681E.
- 44 11. Jiao, Y.; Niu, L.-n.; Ma, S.; Li, J.; Tay, F. R.; Chen, J.-h., Quaternary ammonium-based

- 1 biomedical materials: State-of-the-art, toxicological aspects and antimicrobial resistance. *Prog. Polym.*
- 2 *Sci.* **2017,** *71*, 53-90, DOI:10.1016/j.progpolymsci.2017.03.001.
- 3 12. Yang, R.; Moni, P.; Gleason, K. K., Ultrathin Zwitterionic Coatings for Roughness-Independent
- 4 Underwater Superoleophobicity and Gravity-Driven Oil-Water Separation. Adv. Mater. Interfaces 2015,
- 5 2 (2), 1400489, DOI:10.1002/admi.201400489.
- 6 13. Bamford, C. H.; White, E. F. T., Tertiary amines as chain-transfer agents and their use in the
- 7 synthesis of block copolymers. Transactions of the Faraday Society 1956, 52 (0), 716-727,
- 8 DOI:10.1039/TF9565200716.
- 9 14. Khlyustova, A.; Yang, R., Initiated Chemical Vapor Deposition Kinetics of Poly(4-aminostyrene).
- 10 Front. Bioeng. Biotechnol. **2021**, *9*, 670541, DOI:10.3389/fbioe.2021.670541.
- 11 15. Kuba, A. G.; Smolin, Y. Y.; Soroush, M.; Lau, K. K. S., Synthesis and integration of poly(1-
- 12 vinylimidazole) polymer electrolyte in dye sensitized solar cells by initiated chemical vapor deposition.
- 13 Chem. Eng. Sci. **2016**, 154, 136-142, DOI:10.1016/j.ces.2016.05.007.
- 14 16. Chen, P.; Zhang, Z.; Rouse, Z.; Baker, S. P.; Yeo, J.; Yang, R., Engineering solvation in
- 15 initiated chemical vapour deposition for control over polymerization kinetics and material properties.
- *Nature Synthesis* **2023**, *2* (4), 373-383, DOI:10.1038/s44160-023-00242-5.
- 17 17. Nakabayashi, K.; Mori, H., Recent progress in controlled radical polymerization of N-vinyl
- 18 monomers. Eur. Polym. J. **2013**, 49 (10), 2808-2838, DOI:10.1016/j.eurpolymj.2013.07.006.
- 19 18. Deboudt, K.; Delporte, M.; Loucheux, C., Copolymers of N-vinyl-2-pyrrolidone and 2-
- 20 (dimethylamino)ethyl methacrylate, 1. Synthesis, characterization, quaternization. Macromol. Chem.
- 21 Phys. **1995**, 196 (1), 279-290, DOI:10.1002/macp.1995.021960119.
- 22 19. Santanakrishnan, S.; Hutchinson, R. A., Free-Radical Polymerization of N-Vinylimidazole and
- Quaternized Vinylimidazole in Aqueous Solution. Macromol. Chem. Phys. 2013, 214 (10), 1140-1146,
- 24 DOI:10.1002/macp.201300044.
- 25 20. Bamford, C. H.; Schofield, E., Non-classical free-radical polymerization: Degradative addition to
- 26 monomer in the polymerization of 1-vinylimidazole. Polymer 1981, 22 (9), 1227-1235,
- 27 DOI:10.1016/0032-3861(81)90138-5.
- 28 21. Fan, B.; Wan, J.; McKay, A.; Qu, Z.; Thang, S. H., Facile synthesis of well-controlled poly(1-
- 29 vinyl imidazole) by the RAFT process. *Polym. Chem.* **2020**, *11* (35), 5649-5658,
- 30 DOI:10.1039/D0PY00985G.
- 31 22. Pamedytytė, V.; Abadie, M. J. M.; Maku š ka, R., Photopolymerization of N,N-
- 32 dimethylaminoethylmethacrylate studied by photocalorimetry. J. Appl. Polym. Sci. 2002, 86 (3), 579-
- 33 588, DOI:10.1002/app.10892.
- 34 23. Chen, P.; Lang, J.; Zhou, Y.; Khlyustova, A.; Zhang, Z.; Ma, X.; Liu, S.; Cheng, Y.;
- 35 Yang, R., An imidazolium-based zwitterionic polymer for antiviral and antibacterial dual functional
- 36 coatings. Sci. Adv. 2022, 8 (2), eabl8812, DOI:10.1126/sciadv.abl8812.
- 37 24. Khlyustova, A.; Kirsch, M.; Yang, R., Amphiphilic Copolymer Thin Films with Short Fluoroalkyl
- 38 Side Chains for Antibiofilm Properties at the Solid-Liquid-Air Interface. ACS Sustainable Chemistry &
- 39 Engineering **2022**, 10 (48), 15699-15713, DOI:10.1021/acssuschemeng.2c03933.
- 40 25. Prasath, V. S.; Lau, K. K. S., Kinetically Limited Bulk Polymerization of Polymer Thin Films by
- 41 Initiated Chemical Vapor Deposition. *Macromolecules* **2023**, 56 (24), 10111-10118,
- 42 DOI:10.1021/acs.macromol.3c01868.
- 43 26. Pekel, N.; Şahiner, N.; Güven, O.; Rzaev, Z. M. O., Synthesis and characterization of N-
- 44 vinylimidazole–ethyl methacrylate copolymers and determination of monomer reactivity ratios. Eur.

- 1 *Polym. J.* **2001,** *37* (12), 2443-2451, DOI:10.1016/S0014-3057(01)00124-0.
- 2 27. Dambatta, B. B.; Ebdon, J. R., Kinetic studies of free-radical polymerizations of I-vinylimidazole
- 3 initiated by benzoyl peroxide and azoisobutyronitrile. Eur. Polym. J. 1986, 22 (10), 783-786,
- 4 DOI:10.1016/0014-3057(86)90016-9.
- 5 28. O'Hanlon, J. F., In *A User's Guide to Vacuum Technology*, John Wiley & Sons: 2003.
- 6 29. Yang, H.; Neefjes, I.; Tikkanen, V.; Kubečka, J.; Kurtén, T.; Vehkamäki, H.; Reischl, B.,
- 7 Collision-sticking rates of acid-base clusters in the gas phase determined from atomistic simulation and
- 8 a novel analytical interacting hard-sphere model. Atmos. Chem. Phys. 2023, 23 (10), 5993-6009,
- 9 DOI:10.5194/acp-23-5993-2023.
- 10 30. Zhang, X.; Zhou, S.; Leonik, F. M.; Wang, L.; Kuroda, D. G., Quantum mechanical effects in
- 11 acid-base chemistry. Chem. Sci. 2022, 13 (23), 6998-7006, DOI:10.1039/D2SC01784A.
- 12 31. Kanzaki, R.; Doi, H.; Song, X.; Hara, S.; Ishiguro, S.-i.; Umebayashi, Y., Acid-Base
- 13 Property of N-Methylimidazolium-Based Protic Ionic Liquids Depending on Anion. J. Phys. Chem. B
- **2012**, *116* (48), 14146-14152, DOI:10.1021/jp308477p.
- 15 32. Kim, J. H.; Shin, D. S.; Han, M. H.; Kwon, O. W.; Lee, H. K.; Lee, S. G.; Ghim, H. D.;
- Park, J. M.; Han, S. S.; Noh, S. K.; Lyoo, W. S., Surface free energy analysis of poly(vinyl alcohol)
- 17 films having various molecular parameters. J. Appl. Polym. Sci. 2007, 105 (2), 424-428,
- 18 DOI:10.1002/app.26010.
- 19 33. Torres, J. M.; Stafford, C. M.; Vogt, B. D., Impact of molecular mass on the elastic modulus of
- 20 thin polystyrene films. *Polymer* **2010**, *51* (18), 4211-4217, DOI:10.1016/j.polymer.2010.07.003.
- 21 34. Abiad, M. G.; Carvajal, M. T.; Campanella, O. H., A Review on Methods and Theories to Describe
- the Glass Transition Phenomenon: Applications in Food and Pharmaceutical Products. Food Engineering
- 23 Reviews **2009**, 1 (2), 105-132, DOI:10.1007/s12393-009-9009-1.
- 24 35. Brandrup, J.; Immergut, E. H.; Grulke, E. A.; Abe, A.; Bloch, D. R., Polymer Handbook (4th
- 25 Edition). John Wiley & Sons.
- 26 36. Odian, G., Radical Chain Polymerization. In *Principles of Polymerization*, 2004; pp 198-349.
- 27 37. Chan, K.; Gleason, K. K., A Mechanistic Study of Initiated Chemical Vapor Deposition of Polymers:
- Analyses of Deposition Rate and Molecular Weight. *Macromolecules* **2006**, *39* (11), 3890-3894,
- 29 DOI:10.1021/ma051776t.

30

Curbing Chain Transfer in initiated Chemical Vapor Deposition (iCVD) via Molecular Vapor Complexation

Pengyu Chen^a, Zheyuan Zhang^a, Kwang-won Park^a, Christina H Yu^b, Rong Yang^{a,*}

Supplementary Discussion

Derivation of deposition kinetics involving chain transfer to the imidazole group

Under typical iCVD conditions, the BET isotherm is written as:

$$[M] = \frac{\rho_M}{MW_M} \times c \times P_M / P_{M,sat}$$

where [M] (mol/m³) is the concentration of surface-adsorbed monomers; ρ_M is the density of liquid monomer; MW_M is the molecular weight of monomer; c is the BET constant that describes the enthalpy of a monolayer physisorption. Therefore, the surface monomer concentration is linear to the experimental parameters, $P_M/P_{M,sat}$:

$$P_M/P_{M,sat} \sim [M] \tag{1}$$

where the $P_M/P_{M,sat}$ is the partial pressure of the monomer over the saturation pressure of the monomer under the stage temperature.

For the heterogeneous free-radical polymerization at the interface, there are five elementary reactions as follows:

- (1) Initiation: $R \cdot +M \rightarrow M \cdot$ with an initiation rate constant of f.
- (2) Propagation: $M_n \cdot + M \to M_{n+1}$ with a polymerization rate constant of k_p .
- (3) Degradative addition: $M_n \cdot + M \rightarrow D$ with a reaction rate constant of k_d .
- (4) Termination: $M_n \cdot + M_m \cdot \to M_n + M_m$ and $M_n \cdot + M_m \cdot \to M_{n+m}$ with an overall termination rate constant of k_t .
- (5) Termination by "dead" radicals: $M_n \cdot +D \cdot \to M_{n+1}$ with a reaction rate constant of k_{td} .

Under low surface monomer concentration, the initiation rate is proportional to the surface coverage of the monomer. The mass balance for "living" radicals is expressed as follows:

$$\frac{d[M \cdot]}{dt} = f[M] - k_t[M \cdot]^2 - k_{td}[M \cdot][D \cdot] - k_d[M \cdot][M] = 0$$
 (2a)

Conversely, when the surface monomer concentration is high enough to exceed single-layer adsorption,

$$\frac{d[M \cdot]}{dt} = F - k_t [M \cdot]^2 - k_{td} [M \cdot] [D \cdot] - k_d [M \cdot] [M] = 0$$
 (2b)

where F is a constant. The mass balance of the "dead" radicals is

^{a.} Robert Frederick Smith School of Chemical and Biomolecular Engineering, Cornell University, Ithaca, NY, 14853, USA

b. Materials Science and Engineering, Cornell University, Ithaca, NY, 14853, USA

^{*} Corresponding author: ryang@cornell.edu

$$\frac{d[D\cdot]}{dt} = k_d[M\cdot][M] - k_{td1}[M\cdot][D\cdot] = 0 \tag{3}$$

The deposition rate, DR, can be calculated using Rp, as follow:

$$DR = \frac{h_{ml}MW_MR_p}{\rho} = \frac{h_{ml}MW_Mk_p[M \cdot][M]}{\rho}$$
 (4)

where h_{ml} is monolayer thickness; ρ is the density of polymer. Based on (1) (2a), (3) and (4), the DR under low surface concentration is calculated as

$$DR = \frac{h_{ml}MW_{M}R_{p}}{\rho}R_{p} = \frac{h_{ml}MW_{M}k_{d}k_{p}}{\rho k_{t}}[M]^{2} \left\{ \left(1 + \frac{k_{t}}{k_{d}^{2}} \frac{f}{[M]}\right)^{0.5} - 1 \right\}$$

$$\lim_{[M] \to 0} DR = \frac{h_{ml}MW_{M}k_{p}}{\rho k_{t}^{0.5}} \left(\frac{c\rho_{M}}{MW_{M}}\right)^{1.5} f^{0.5} \left(P_{M}/P_{M,sat}\right)^{1.5}$$
(5a)

Similarly, based on (1) (2b), (3) and (4), the *DR* under high surface monomer concentration is calculated as:

$$DR = \frac{h_{ml}MW_{M}k_{d}k_{p}}{\rho k_{t}} [M]^{2} \left\{ \left(1 + \frac{k_{t}}{k_{d}^{2}} \frac{f}{[M]^{2}} \right)^{0.5} - 1 \right\}$$

$$\lim_{[M] \to \infty} DR = \frac{h_{ml}MW_{M}k_{p}}{2\rho k_{d}} f$$
(5b)

Therefore, the deposition rate scales with $P_M/P_{M,sat}$ to the power of 1.5 under sub-monolayer monomer adsorption. It is independent of $P_M/P_{M,sat}$ under multilayer monomer adsorption.

Calculation of monomer surface concentration

The $P_{1VI-AA,sat}$ was extracted from the pressure plateau in Figure 2 (b), giving $P_{1VI-AA,sat}$ =0.21 Torr. Based on the experimental conditions, i.e., the total pressure and flow rates of 1VI and AA, the partial pressure could be calculated using

$$P_A = \frac{P_{tot}F_A}{F_{tot}} \tag{6}$$

where the P_A is the partial pressure of component A; F_A is the flow rate of component A; F_{tot} is the total flow rate.

Based on equilibrium constant (K) between AA and 1VI, P_{1VI-AA} and P_{1VI} could be solved by the following equations:

$$\begin{aligned} P_{VI} + P_{AA} + P_{VI-AA} + P_{others} &= P_{tot} \\ P_{VI-AA} &= K P_{VI} P_{AA} \end{aligned}$$

where P_{others} includes initiator and Argon.

The corrected $P_{IVI}/P_{IVI,sat}$ is approximately estimated as

$$P_{VI}/P_{sat}(corrected) = P_{VI}/P_{VI,sat} + P_{VI-AA}/P_{VI-AA,sat}$$

that gives a correction factor, CF

$$CF = \frac{P_{VI}/P_{sat}(corrected)}{P_{VI}/P_{VI,sat}(w/o\ complexation)}$$

The corrected surface monomer fraction, f', is corrected as

$$f' = \frac{CFf}{CFf + 1 - f}$$

The correction factor and corrected surface monomer fraction are summarized in Table S1:

Correction factor	$f_{IVI}(DVB)$	$f'_{1VI}(DVB)$	$f_{1VI}(V4D4)$	$f'_{1VI}(V4D4)$
3.75±0.02 —	0.90	0.97	0.90	0.97
	0.70	0.90	0.70	0.90
	0.50	0.79	0.60	0.85
	0.30	0.62	0.50	0.79
	0.10	0.29	-	-

Estimation of the glass transition temperature of p1VI

A T_g value of ~131 °C has been reported for p1VI with a molecular weight of 5.3 kDa, much lower than its $T_{g,\infty}$ of ~176 °C. Based on the Flory-Fox equation (with the K value of 157.5 °C·kg/mol), we estimated T_g to be 152 °C for p1VI with a molecular weight of 8.2 kDa (PDI=1.24) and 163°C for a molecular weight of 16.1 kDa (PDI=1.34).

Supplementary Figures

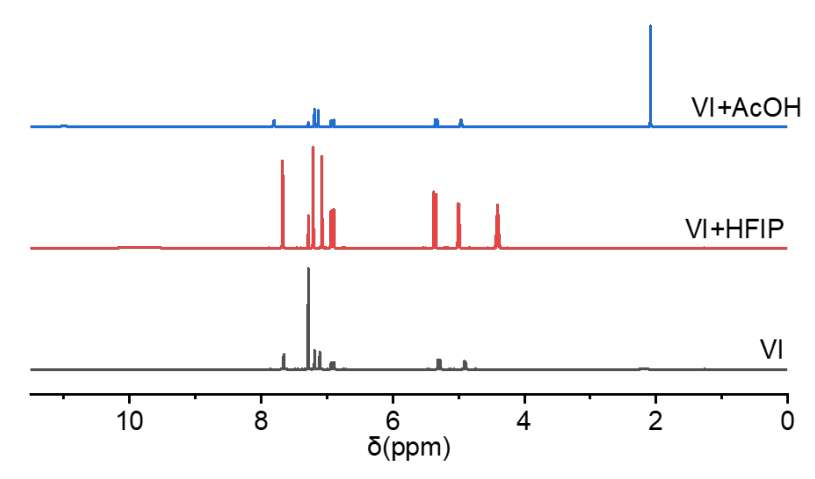


Figure S1. NMR spectra of 1VI, 1VI with HFIP, 1VI with AcOH.

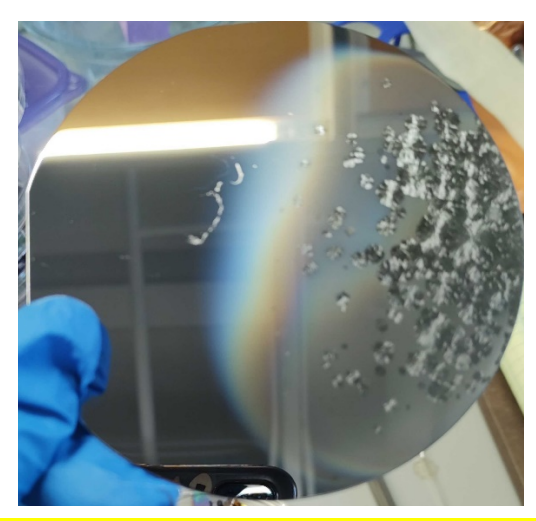


Figure S2. Optical image of the crystalline condensation formed upon introducing a TFA and 1VI co-flow into the reactor chamber.

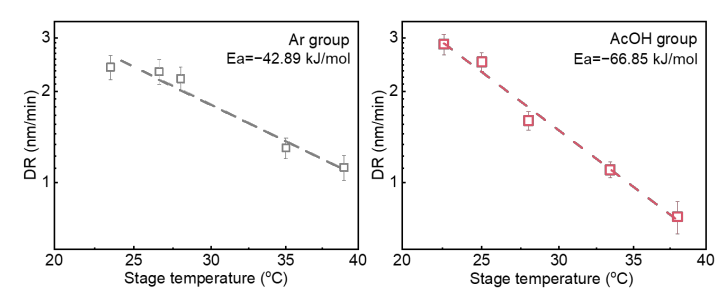


Figure S3. The Arrhenius plot for the iCVD polymerization of 1VI, using Ar or AcOH as the patch flow, revealing distinct temperature dependence.

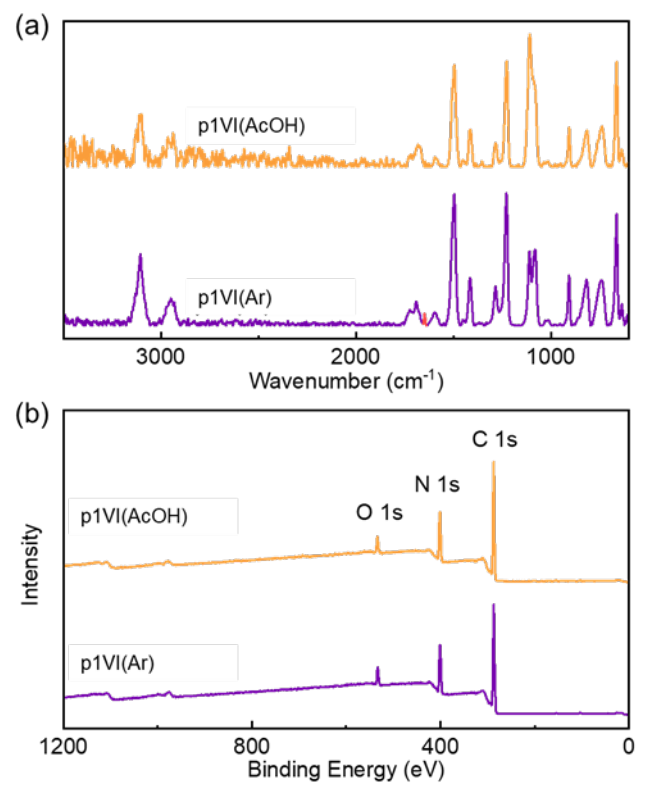


Figure S4. FTIR spectra (a) and XPS survey scan (b) of p1VI deposited using AcOH.

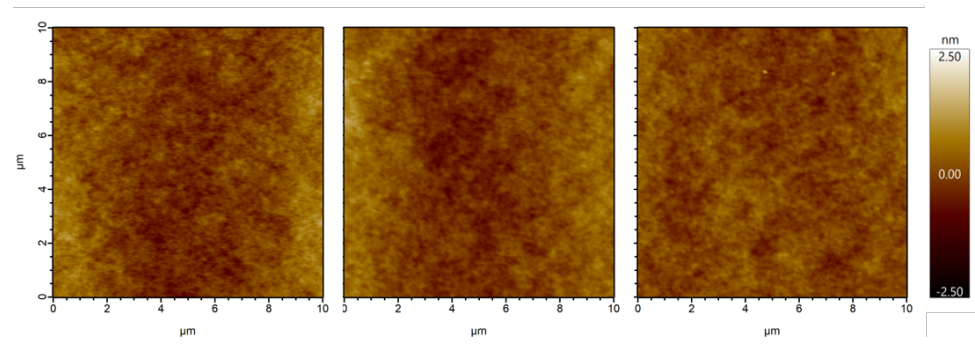


Figure S5. AFM images of p1VI film deposited using Ar (left), 1 sccm AcOH (middle), and 2 cm AcOH (right) showing smooth surfaces.

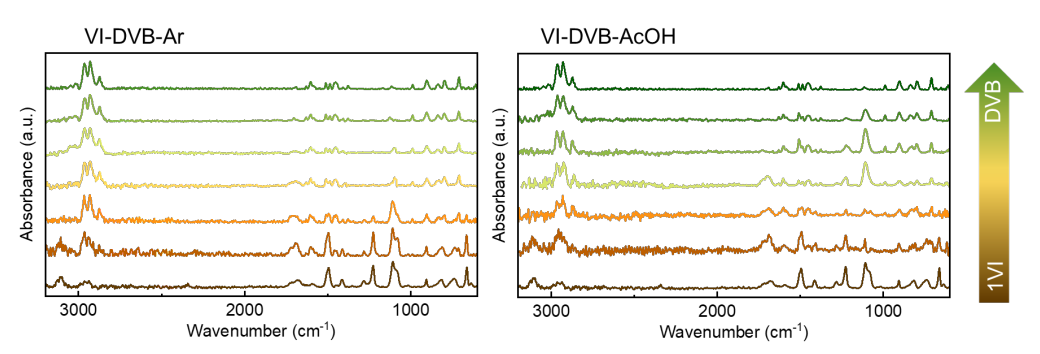


Figure S6. FTIR spectra of p1VI-co-DVB film deposited using Ar or AcOH under different 1VI to DVB ratios (10:0, 8:2, 6:4, 5:5, 4:6, 2:8, 0:10).

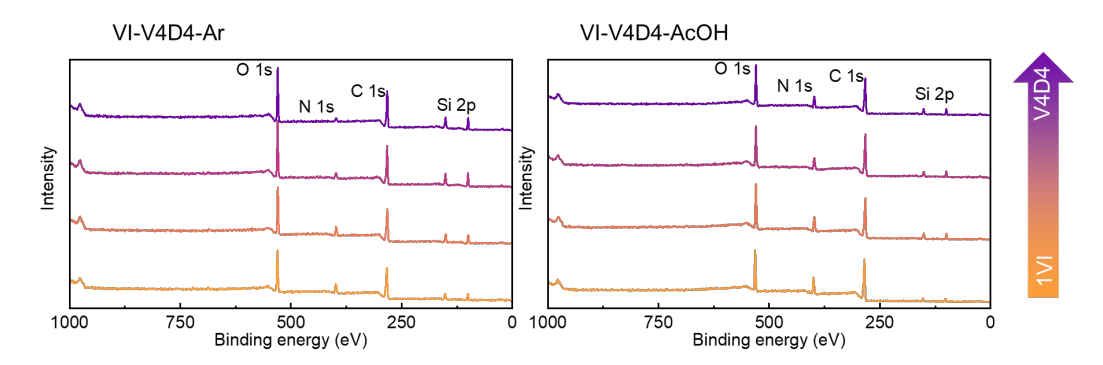


Figure S7. FTIR spectra of p1VI-co-V4D4 film deposited using Ar or AcOH under different 1VI to V4D4 ratios (5:5, 6:4, 7:3, 9:1).

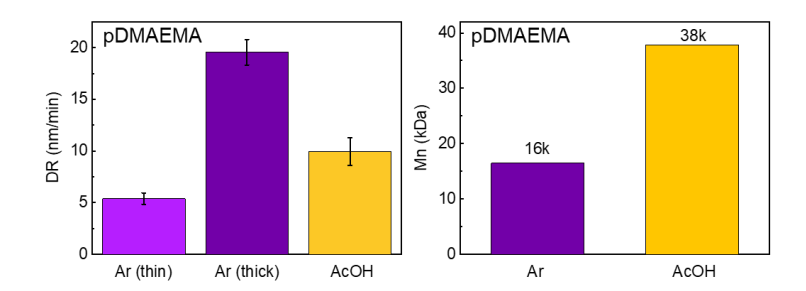


Figure S8. Deposition rates and molecular weight of pDMAEMA deposited using Ar or AcOH.